

Galvanic Deoxidation of Molten Steel using a Solid Electrolyte Cell

by

ZAIN HASHAM

B.S.E., Material Science and Engineering, University of Pennsylvania (1992)
B.S.Econ., Entrepreneurial Management, University of Pennsylvania (1992)

Submitted to the Department of Material Science and Engineering in partial
fulfillment of the requirement for the degree of

Master of Science in Metallurgy


at

MASSACHUSETTS INSTITUTE OF TECHNOLOGY

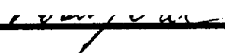
May 1994

© 1994 Massachusetts Institute of Technology. All rights reserved.


Signature of Author _____


Department of Material Science and Engineering
May 6, 1994

Certified by _____


Professor Uday B. Pal
Thesis Supervisor

Accepted by _____


Professor Carl V. Thomson II
Professor of Electronic Materials
Chair, Departmental Committee on Graduate Students

ARCHIVES

MASSACHUSETTS INSTITUTE
OF TECHNOLOGY

AUG 18 1994

GALVANIC DEOXIDATION OF MOLTEN STEEL USING A SOLID ELECTROLYTE CELL

by

ZAIN HASHAM

Submitted to the Department of Material Science and Engineering on May 6, 1994 in partial fulfillment of the requirement for the degree of Master of Science in Metallurgy

ABSTRACT

Galvanic deoxidation of steel is investigated. The inner walls of one-end-closed yttria stabilized zirconia tube is coated with molybdenum-zirconia cermet. A reducing gas of hydrogen is passed through the tube. The zirconia tube is dipped into the induction stirred steel melt, and the cermet is short circuited with the melt. The oxygen chemical potential gradient across the solid electrolyte is used to deoxidize the melt. The external short circuit current can be divided into two zones which are characterized by total resistance control and mass transport control respectively. The external short circuit current is used to model the deoxidation process.

Thesis Supervisor: Professor Uday B. Pal

Title : John Chipman Assistant Professor of Chemical Processing of Materials

TABLE OF CONTENTS

TITLE PAGE	1
ABSTRACT	2
TABLE OF CONTENTS	3
LIST OF SYMBOLS	4
LIST OF FIGURES	6
LIST OF TABLES	7
ACKNOWLEDGMENTS	8
1. INTRODUCTION	9
2. LITERATURE RESEARCH	12
3. EXPERIMENTAL APPARATUS	17
4. THEORETICAL ASPECTS	22
5. RESULTS AND DISCUSSION	28
6. SUMMARY AND CONCLUSION	45
APPENDIX A	46
APPENDIX B	49
BIBLIOGRAPHY	51
BIOGRAPHICAL NOTE	53

LIST OF SYMBOLS

Symbol	Description	Units
A	Electrolyte/melt interfacial area	m ²
C _o	Initial oxygen concentration in steel melt	ppm
C _b	Bulk oxygen concentration in the melt	ppm
C _i	Oxygen concentration at the melt/electrolyte interface	ppm
C _r	Oxygen concentration in the reducing gas	ppm
d	Thickness of zirconia tube	m
D	Diffusivity of oxygen in steel melt	m ² /s
F	Faraday constant (96485)	col./eqv.
E _n	Nernst potential	Volts
E _m	Open circuit EMF	Volts
I _{ion}	Ionic current through electrolyte under short circuit conditions	A
I _e	Electronic current through electrolyte under short circuit condition	A
I _{ex}	External short circuit current	A
I' _{ion}	Ionic current through electrolyte under open circuit condition	A
I' _e	Electronic current through electrolyte under open circuit conditions	A
J	Oxygen flux in the melt	ppm. m/s
M _{melt}	Mass of steel melt	kg
M _o	Mass of one mole oxygen atom	kg
N _{H2(i)}	Flow rate of hydrogen gas in refining device	moles/min
N _{O2(i)}	Initial number of moles of oxygen gas present in the reducing gas	moles/min
N _{H2O(i)}	Initial number of moles of water vapor present in the reducing gas	moles/min
N _{O2(s.c.)}	Number of moles of oxygen gas entering the reducing gas due to short circuiting the refining device	moles/min
K _s	Sievert's law constant	ppm.atm ^{-1/2}

Symbol	Description	Units
K_p	Equilibrium constant for the reaction between hydrogen and oxygen gas	
$P_{O_2}^i$ (melt)	Oxygen partial pressure at the melt/electrolyte interface	atm
$P_{O_2}^r$ (red. gas)	Oxygen partial pressure in the reducing gas	atm
R_{total}	Total resistance of the short circuited electrolyte cell	ohms
R_e	Electronic resistance of the electrolyte cell	ohms
R_{ex}	External resistance	ohms
R_{ion}	Ionic resistance of the electrolyte cell	ohms
R	Gas constant (8.314)	J/K-mole
T	Temperature of steel melt	K
T_2	Room temperature	K
t_{ion}	Ionic transport number of electrolyte	
V	Flow rate of the reducing gas	m^3/min
α	Mass transfer coefficient	m/s
δ	Thickness of diffusion boundary layer	m
ΔC	Difference in oxygen concentration between the bulk and melt/electrolyte interface	ppm
σ_{ion}	Ionic conductivity of the zirconia tube	$(ohm\ m)^{-1}$
σ_e	Electronic conductivity of the zirconia tube	$(ohm\ m)^{-1}$
ρ_{melt}	Density of the melt	kg/m^3

LIST OF FIGURES

Figure	Description	Page
<u>Fig 1</u>	Principal involved in the deoxidation process	11
<u>Fig 2</u>	Equivalent circuit representing short circuited refining device	15
<u>Fig 3</u>	Schematic representation of experimental apparatus	18
<u>Fig 4</u>	Flow chart for preparing cermet	20
<u>Fig 5</u>	Schematic representation of steps involved in the deoxidation process	23
<u>Fig 6</u>	Plot of $\text{Ln}(I_{\text{ext}})$ vs. time for experiment A	33
<u>Fig 7</u>	Plot of $\text{Ln}(I_{\text{ext}})$ vs. time for experiment B	34
<u>Fig 8</u>	Plot of $\text{Ln}(I_{\text{ext}})$ vs. time for experiment C	35
<u>Fig 9</u>	Plot of $\text{Ln}(I_{\text{ext}})$ vs. time for experiment D	36
<u>Fig 10a</u>	External current vs. time curve for Experiment A	37
<u>Fig 10b</u>	Ionic current vs. time curve for Experiment A	37
<u>Fig 11a</u>	External current vs. time curve for Experiment B	38
<u>Fig 11b</u>	Ionic current vs. time curve for Experiment B	38
<u>Fig 12a</u>	External current vs. time curve for Experiment C	39
<u>Fig 12b</u>	Ionic current vs. time curve for Experiment C	39
<u>Fig 13a</u>	External current vs. time curve for Experiment D	40
<u>Fig 13b</u>	Ionic current vs. time curve for Experiment D	40
<u>Fig 14</u>	Oxygen concentration vs. time curve for Experiment A	41
<u>Fig 15</u>	Oxygen concentration vs. time curve for Experiment B	42
<u>Fig 16</u>	Oxygen concentration vs. time curve for Experiment C	43
<u>Fig 17</u>	Oxygen concentration vs. time curve for Experiment D	44

LIST OF TABLES

	Description	Page
Table 1	Deoxidation experimental parameters and calculated mass transfer coefficients	32

ACKNOWLEDGMENTS

I would like to thank the following people for the help and the advice that they have given me:

Prof. U.B.Pal (Thesis Supervisor), Prof. Worrell (Univ. of Pennsylvania), Prof. K.C.Chou (Univ. of Science and Technology, Beijing), Prof. Li (University of Science and Technology, Beijing), Dr. Krishna Murthy, Shi Yuan, Filippos Patsiogiannis, Sridhar Seetharaman, Karl Cheng, and Steve Britten.

I would like to thank the Ministry of Science and Technology, Islamabad, Pakistan, for providing me with a scholarship for my education at Massachusetts Institute of Technology.

I would also like to thank US Steel (a division of USX Corporation) for providing steel samples.

In addition, I would like to thank the National Science Foundation (NSF) for funding this research project.

CHAPTER 1

INTRODUCTION

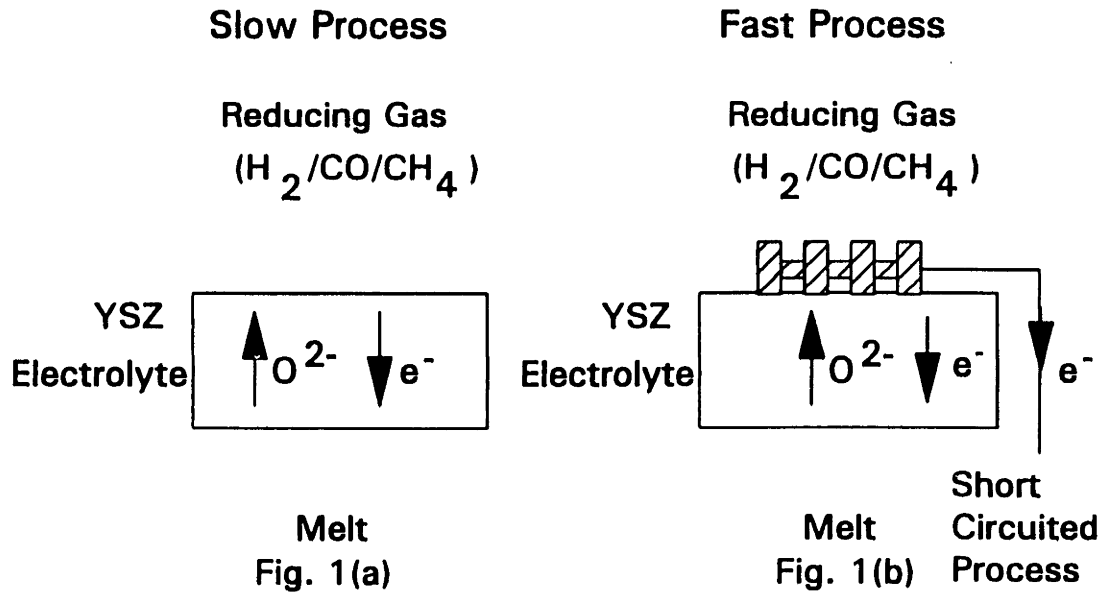
As the demand for metals with superior physical and mechanical properties has increased, it has resulted in the search for new metal refining techniques capable of reducing the concentration of undesirable elements like hydrogen (H), oxygen (O) and sulfur (S) to very low levels. Currently the two most popular metal refining techniques include vacuum degassing and addition of reagents to form stable compounds with the undesirable elements. However, the former technique is capital intensive and is limited by the vacuum pressure which can be created over the melt. In the latter technique, some of the reagent metals can be very expensive, and the compounds of the undesirable elements, if not completely removed, may remain as inclusions in the metal. In addition, the reagent goes into solution in the melt, which may not be desirable. In this thesis we have investigated a new electrochemical refining technique for removing oxygen from molten steel.

This technique consists of inserting a yttria stabilized zirconia (YSZ) tube (one end closed) into a steel bath, thus exposing the outside of the YSZ tube to the steel bath, while a reducing gas (with low partial pressure of oxygen) is blown inside the tube. As yttria stabilized zirconia is an oxygen ion conductor [1-6], the oxygen chemical potential gradient across the electrolyte will result in the migration of oxygen ions from the steel melt, into the reducing gas (to satisfy electroneutrality, the electrons must migrate in the opposite direction). The melt is stirred by induction stirring. In this way, the metal can be deoxidized, without allowing the reducing gas to come into direct contact with the metal. In addition, the inside of the YSZ tube is coated with a porous molybdenum-zirconia cermet, and this cermet is short circuited with the steel melt. The purpose of short circuiting the molybdenum-zirconia cermet is to provide an alternative path for the

migration of electrons from the zirconia tube to the melt. As YSZ is predominantly an ionic conductor, its electronic transport number is rather small [7-10]. Therefore, by short circuiting the YSZ tube with the melt, the rate of oxygen extraction can be increased, and the current in the external circuit can be analyzed to model the deoxidation process. The principle involved in this deoxidation process is schematically represented in Fig 1a and 1b.

Some of the advantages of the new refining technique are listed below:

- 1) Practically no harmful by-products in the form of dust, gas or slag are generated.
- 2) The refining device operates as a galvanic (current producing) cell, and therefore no external EMF source is necessary. This refining technique is thus more energy efficient as it converts chemical energy directly into electrical energy.
- 3) The reactants and by-products are gaseous and hence no inclusions form inside the melt.
- 4) Reducing gases containing H_2 , CH_4 and CO can be used to refine the metal without running the risk of increasing the H or C content of the metal.



CHAPTER 2

LITERATURE RESEARCH

Korousic and Marincek [11] in 1968, were among the first few to do research in deoxidizing molten metal using a solid electrolyte. In their experiment, they used a hollow one end closed, magnesia- stabilized zirconia tube which contained molten copper. This tube was immersed in a crucible containing copper melt. Molybdenum rods were immersed in the copper melt inside and outside the zirconia tube, and an external EMF was applied to drive the oxygen from the copper melt inside the zirconia tube, to the copper melt outside the zirconia tube. The purpose of their experiment was to demonstrate the feasibility of using the oxygen ion conducting property of stabilized zirconia to extract oxygen from molten metal.

In 1972, Fisher and Janke [12] used an external EMF to deoxidize a steel bath. In their experiment, they used a stabilized zirconia tube (one end closed) which was immersed into a molten steel bath. A noble metal/gas electrode, or a liquid metal electrode with a graphite contact rod was used as the anode. A metal lead wire inserted into the molten steel bath served as the cathode, and an external EMF was applied to deoxidize the steel melt. The steel melt was stirred by mechanical means. Fisher and Janke found in their experiment that the rate of deoxidation of the melt remained constant between oxygen concentrations of 0.047 and 0.016%. However, below oxygen concentration of 0.016%, the rate of deoxidation of the melt decreased with oxygen content. Therefore, they concluded that the O^{2-} ion transport through the solid electrolyte was the rate controlling step in the oxygen concentration range of 0.047-0.016%. But, below an oxygen concentration of 0.016% the rate controlling step was the diffusion of oxygen ions from the melt to the melt/zirconia interface.

In 1973, Oberg et.al. [13] did a similar experiment on copper melts, i.e. used an external EMF to deoxidize copper. Their experimental set up consisted of a calcia stabilized zirconia crucible which contained the copper melt. The outside of this crucible was coated with platinum and was exposed to air. The platinum served as the anode, while the copper melt served as the cathode. The melt was stirred by induction stirring and an external EMF was then applied to drive the dissolved oxygen from the copper melt, through the solid electrolyte, into the air. Oberg et. al. concluded that the rate controlling step for the deoxidation reaction was the transport of oxygen in the electrolyte at higher oxygen concentrations in the melt (> 90 ppm), and transport across a boundary layer in the melt at the melt/ electrolyte interface when the oxygen concentration in the melt was below 45 ppm.

One of the problems associated with using an external EMF to deoxidize the melt is dissociation of the electrolyte [13]. If high external EMF is used, the oxygen concentration at the melt/electrolyte interface will become very low, and this will result in the decomposition of the electrolyte. In addition, if this method is used at high temperature (e.g. steel making temperatures), the high electronic conductivity of the electrolyte appreciably decreases the current efficiency. For calcia stabilized zirconia (CSZ) the current efficiency is reported to be around 30% when the oxygen concentration in the steel melt is below 300 ppm [14-15].

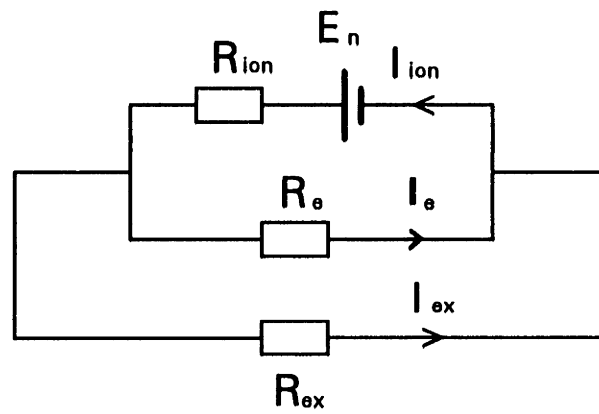
Therefore, in view of the above mentioned problems, in 1981 Iwase et.al. [16] proposed a galvanic method for deoxidizing steel using a solid electrolyte. In their experiment, they inserted an one end closed CSZ tube into a molten steel bath (1823 K) contained in an alumina crucible, and passed a mixture of CO/CO₂ through the tube. At around 1823 K, the residual electronic conductivity in CSZ allows the electrons and oxygen ions to migrate in opposite directions under an oxygen chemical potential gradient. This way the steel is deoxidized. However, the residual electronic conductivity decreases exponentially as the temperature is lowered and therefore this technique is not suitable for

deoxidizing molten metals at lower temperatures such as copper. Iwase et.al. stirred the steel melt by bubbling argon during the deoxidation experiments. They found that when the oxygen concentration in the steel melt was in the range of 580-200 ppm, the rate controlling step was the transport of oxygen across a boundary layer in the melt at the melt/electrolyte interface. This result is different from the one that Fisher et.al. [12] obtained. The reason for this is that in Iwase's experiment the stirring intensity of the melt was lower and therefore the mass transfer coefficient of oxygen in the melt was smaller.

In the experiment described in this thesis, a YSZ tube (one end closed) is coated inside with a Mo-ZrO₂ cermet electrode. A reducing gas is passed through the tube, the cermet electrode is electrically short circuited (externally) to an inductively stirred steel melt and the tube is dipped into the steel melt. The chemical potential gradient of oxygen across the YSZ electrolyte tube is used to deoxidize the steel melt (i.e. no external EMF is utilized). However, these experiments are different from the experiments performed by Iwase et.al [16].

The major differences are listed below:

1. By externally short circuiting the Mo-ZrO₂ cermet and the steel melt, this process does not rely on the residual electronic conductivity of the zirconia for oxygen migration (Fig. 1). As a result this deoxidation process is faster and it can also be used at lower temperatures.
2. The equivalent electrical circuit representing the deoxidation process is shown in Fig. 2. The external (short circuit) current generated during the deoxidation process is a very accurate real time analytical tool that can be used for modeling the deoxidation process. Iwase et.al. relied on the oxygen analysis of the pin samples to model the deoxidation process and that interrupted the thermal and mass balance of the system.
3. Induction stirring was used instead of argon bubbling and as a result the mass transfer coefficient was higher and the deoxidation process was much faster.
4. The initial oxygen concentration in the steel melt was below 670 ppm and therefore the

FIGURE 2

$$I_{ex} + I_e = I_{ion}$$

$$R_{total} = R_{ion} + \frac{R_e \times R_{ex}}{R_e + R_{ex}}$$

$$I_{ion} = \frac{E_n}{R_{total}}$$

$$I_{ion} = I_{ex} \left(\frac{R_e + R_{ex}}{R_e} \right)$$

hercynite phase did not form. At 1873 K, the hercynite phase forms when the oxygen concentration in the melt is over 750 ppm [17]. In the experiments conducted by Iwase et. al., the hercynite phase formed. The formation of the hercynite phase could complicate the interpretation of the deoxidation process because it can dissociate as the melt is deoxidized.

CHAPTER 3

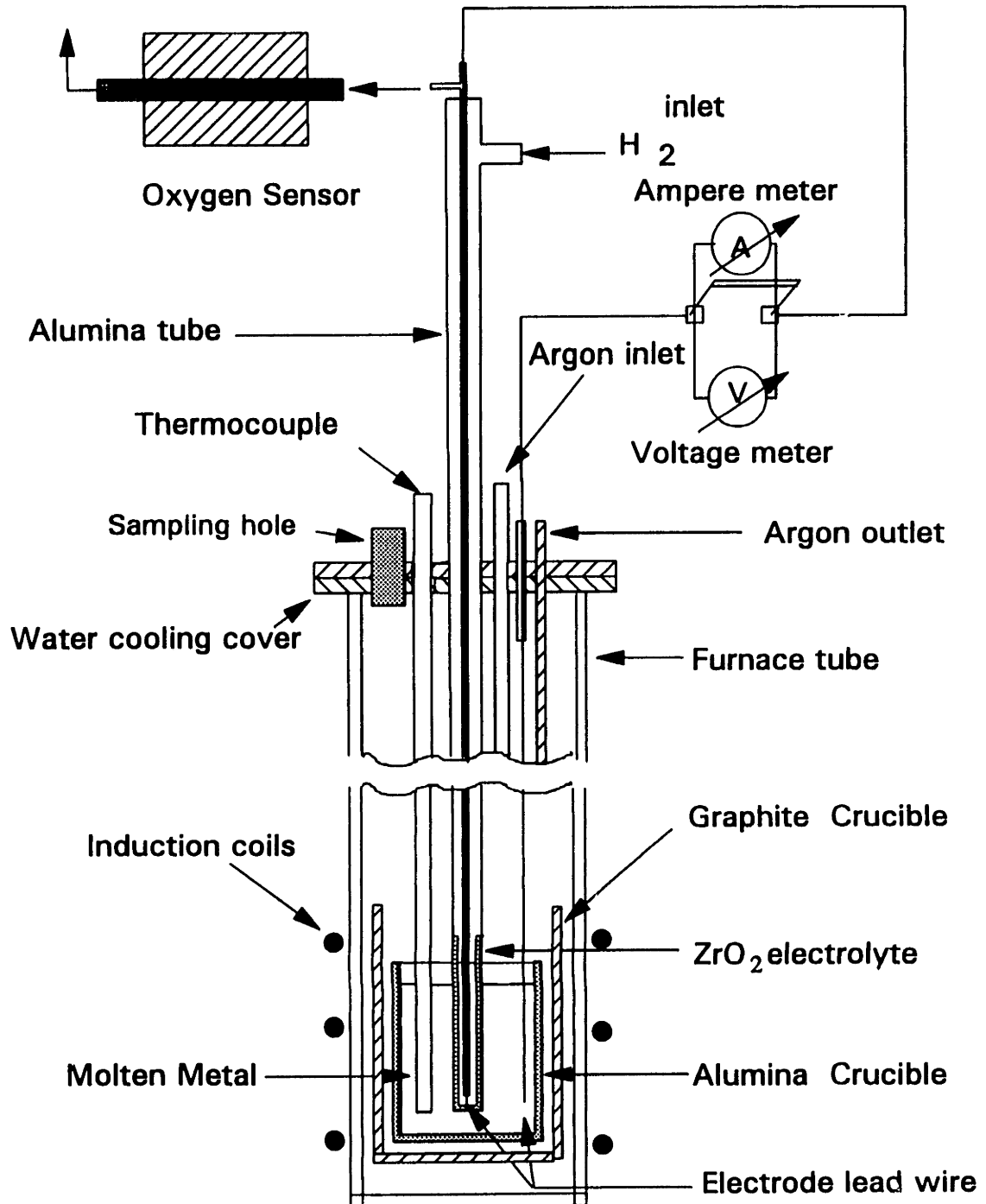
EXPERIMENTAL APPARATUS

The schematic of the experimental apparatus used in these deoxidation experiments is shown in Fig 3. An alumina crucible containing 0.7-0.8 kilograms of low carbon steel is placed inside a graphite crucible which is then placed inside an alumina furnace tube. This furnace tube is sealed using a water cooled brass cooling plate and is placed inside the coils of an induction furnace. The graphite crucible is thin walled (3.8×10^{-3} m) and as a result it allows some amount of induction stirring in the steel melt. At the same time, the graphite crucible evens out the temperature gradient in the inner alumina crucible (containing the steel melt) and prevents it from cracking.

The water cooled brass plate contains six openings. Five of these openings are for argon gas inlet, argon gas outlet, thermocouple (S-type, Pt-10% Rh vs. Pt) which is enclosed in a one end closed alumina sheath, electrode lead wire and refining device. The last opening is used for taking out molten steel samples for analysis.

The refining device consists of a one-end-closed 8 weight % yttria stabilized zirconia tube (length = 0.089 m, OD = 0.0127 m, ID = 9.525×10^{-3} m). The inside of the YSZ tube is coated with a molybdenum-zirconia slurry and is allowed to dry for 24 hours. The slurry is made by mixing 58.32 weight % Mo (Johnson Matthey, 99.9% pure), 14.72 weight % yttria stabilized zirconia (TOSOH, TZ-8Y), and 27.19 weight % PVA (poly vinyl alcohol) solution. The slurry coated zirconia tube is then heated to 1473 K in an environment of hydrogen gas (flow rate = 120 ml/min) and argon gas (flow rate =500

Fig 3: Experimental Apparatus



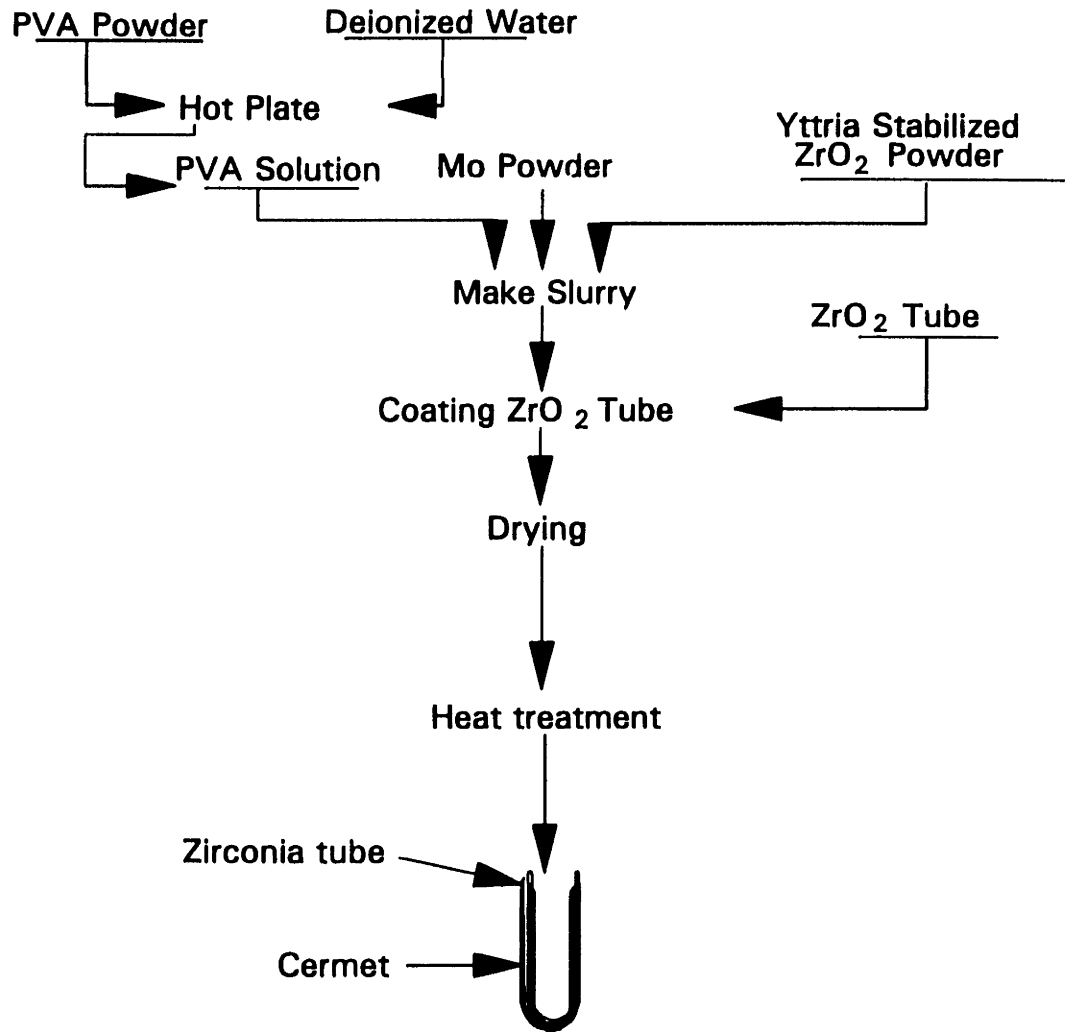
ml/min) and held for 1 hour. The flow chart representing the steps involved in the making of the cermet is shown in Fig 4.

The open end of the cermet coated zirconia tube is then sealed to an open ended alumina tube by a ceramic adhesive (Ultra-Temp 516, Aremco Products, Inc.). The sealing process involves applying the adhesive, heating for 8 hours at 363 K and then heating for 1 hour at 523 K. This process is then repeated until the joint between the zirconia tube and the alumina tube becomes gas tight. Cement (X-9 Plaster from Crucible Refractory Co.) is also applied to increase the strength of the sealing. The gas tightness of the entire refining device is then measured with a vacuum pump (Nalgene, Neward Enterprises).

The inside of the refining device is flushed with reducing gas (99.9% H₂ , Matheson Gas Company). Flowrates of 200 - 300 ml/min are used. The oxygen partial pressure in the reducing gas exiting the refining device is monitored with an oxygen sensor (ZIRCOA, type AACC). A molybdenum wire is sintered to the molybdenum-zirconia cermet and is connected to one of the terminals of a bi-polar switch. The other terminal of the switch is connected to the electrode lead wire which dips into the molten steel. This lead wire is made by mixing La_{0.84}Sr_{0.16}CrO₃ powder (Seattle Specialty Ceramics) with 6% PVA solution and compressing it around a molybdenum wire using an isostatic pressure of 40,000 psi for 5 minutes. The purpose of the 6 % PVA solution is to act as a binder. In addition, the electrode lead wire is sintered during the experiment by holding it 0.01 m above the melt for 20 minutes before it is immersed into the steel melt.

During the experiment, the low carbon steel is melted in the induction furnace. The molten steel is maintained in an inert atmosphere of argon gas with a trace of forming gas (3000 ml/min of Ar + 100 ml/min of forming gas). Forming gas is a mixture of 95% N₂ and 5% H₂ . The partial pressure of oxygen in the gas above the steel melt is found to correspond to 550 ppm of oxygen. By taking several steel samples before inserting the

Fig 4: Steps involved in the making of the Cermet



refining device into the melt, it is verified that the gas environment above the melt is not causing any deoxidation of the melt.

Once the refining device is inserted into the melt, the bi-polar switch can be operated either in the open circuit mode, in which case it will read the electrolyte cell voltage, or it can be operated in the short circuit mode, in which case it will read the short circuit external current. At the end of the experiment, another steel sample is taken in order to find out the final oxygen concentration in the melt.

CHAPTER 4

THEORETICAL ASPECTS

As illustrated in Fig 5, the steps involved in the deoxidation process include:

- 1) transport of oxygen dissolved in the melt, from the bulk metal to the melt/electrolyte interface.
- 2) electrode reaction at the melt/electrolyte interface : $\underline{O} \text{ (melt)} + 2e^- \rightarrow O^{2-}$
- 3) diffusion of oxygen ions through the electrolyte to the electrolyte/reducing gas interface.
- 4) electrode reaction at the electrolyte/reducing gas interface:
 $O^{2-} \rightarrow 2e^- + (1/2)O_2(g)$
- 5) diffusion of oxygen molecules through the porous electrode into the bulk of the reducing gas.

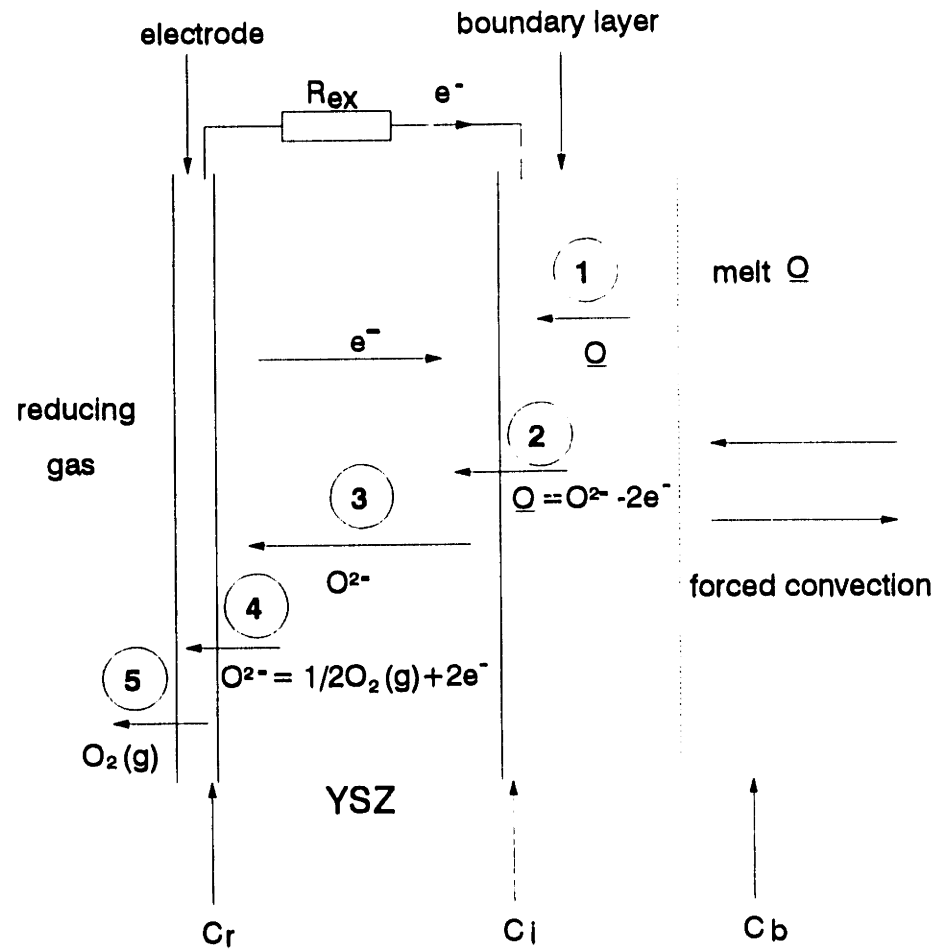
Under conditions of high temperature and relatively small current densities (0.5-2.5 mA/cm²), steps 2,4 and 5 are known to be very rapid, and therefore not rate controlling [18]. Hence, the two steps which are likely to be rate controlling are oxygen diffusion in the melt (step 1), and/or transport of oxygen in the electrolyte (step 3).

The equivalent circuit for the deoxidation process is shown in Fig 2. According to this circuit, it is apparent that the total resistance of the solid electrolyte cell can be divided into three parts: the ionic resistance R_{ion} (ohm), the electronic resistance R_e (ohm), and the external resistance R_{ex} (ohm). Therefore, from this equivalent circuit the total resistance R_{total} (ohm) is equal to,

$$R_{total} = R_{ion} + \frac{R_e \times R_{ex}}{R_e + R_{ex}} \quad [3]$$

where $R_{ion} = \frac{d}{\sigma_{ion} \times A}$,

Fig 5: Steps involved in the Deoxidation Process



d = thickness of the zirconia tube (m), σ_{ion} = ionic conductivity ($\text{ohm}^{-1}\text{m}^{-1}$), and A = interfacial area of electrode/electrolyte (m^2).

According to the Nernst equation,

$$E_n = \frac{RT}{4F} \ln \frac{Po_2^i(\text{melt})}{Po_2^r(\text{red. gas})} \quad [4]$$

where E_n = Nernst Potential (Volts), T = temperature of the steel melt (K), R = gas constant (J/K.mole), $Po_2^i(\text{melt})$ = oxygen partial pressure at the melt/electrolyte interface (atm.), $Po_2^r(\text{red. gas})$ = oxygen partial pressure in the reducing gas (atm.).

Using eq.[3] and eq.[4], the ionic current, I_{ion} (Amperes) can be written as

$$I_{ion} = \frac{E_n}{R_{total}} = \frac{RT}{4F} \frac{\ln \frac{Po_2^i(\text{melt})}{Po_2^r(\text{red. gas})}}{\frac{d}{\sigma_{ion}A} + \frac{R_c \times R_{ex}}{R_c + R_{ex}}} \quad [5]$$

In addition, the diffusion of oxygen across the boundary layer at the melt/electrolyte interface can be described by using Fick's first law. In order to simplify the analysis, all activity coefficients are taken equal to unity.

$$J = -D \frac{\partial C}{\partial x} = -\alpha \times \Delta C \quad [6]$$

where $\alpha = \frac{D}{\delta}$

In the above equation, J = oxygen flux in the melt (ppm. m/s), D = diffusivity of oxygen in the melt (m^2/s), α = mass transfer coefficient of oxygen in steel (m/s), ΔC = difference in

the oxygen concentration between the bulk, and the melt/electrolyte interface (ppm), and δ = thickness of the diffusion boundary layer (m).

Assuming that there is no accumulation of oxygen ions at the melt/electrolyte interface the ionic current can also be represented in terms of the oxygen flux in the melt :

$$I_{\text{ion}} = \frac{2FJA\rho_{\text{melt}}}{M_o \times 10^6} = \frac{2\alpha AF(C_b - C_i)\rho_{\text{melt}}}{M_o \times 10^6} \quad [7]$$

where M_o = mass of oxygen (kg), A = interfacial area of electrode/electrolyte (m^2), ρ_{melt} = density of steel (kg/m^3), C_b = concentration of oxygen in the bulk (ppm), and C_i = concentration of oxygen at the melt/electrolyte interface (ppm).

From mass balance consideration, the following equation will hold:

$$C_b = C_o - \int_0^t \frac{I_{\text{ion}} \times M_o \times 10^6}{2FM_{\text{melt}}} d\zeta \quad [8]$$

where C_o = initial oxygen concentration in the steel melt (ppm), and M_{melt} = mass of the steel melt (kg).

Using Sievert's Law, eq.[5] can be modified to the following form:

$$I_{\text{ion}} = \frac{\frac{RT}{2F} \text{Ln} \frac{C_i(\text{melt})}{C_r(\text{red. gas})}}{R_{\text{total}}} \quad [9]$$

where $C_i(\text{melt})$ = oxygen concentration at the melt/electrolyte interface (ppm), and $C_r(\text{red. gas})$ = oxygen concentration in the reducing gas (ppm).

The relationship between the oxygen concentration, and the partial pressure of oxygen can be represented by the following equations:

$$C_i = K_s(P_{O_2}^i)^{\frac{1}{2}}, \quad C_r = K_s(P_{O_2}^r)^{\frac{1}{2}}$$

where K_s = Sievert's constant. This constant can be calculated from the free energy change of the following reaction:



In this thesis, the free energy data calculated by Elliott et.al [19] is used.

Eq.[9] can be rewritten as:

$$C_i = C_r \exp\left\{\frac{2F[I_{ion}R_{total}]}{RT}\right\} \quad [11]$$

By combining eqs. [7], [8] and [11], the following equation can be derived:

$$C_r \exp\left\{\frac{2F[I_{ion}R_{total}]}{RT}\right\} + \frac{I_{ion}M_o \times 10^6}{2\alpha AF\rho_{melt}} = C_o - \int_0^{\zeta} \frac{I_{ion} \times M_o \times 10^6}{2FM_{melt}} d\zeta \quad [12]$$

Eq. [12] can be differentiated to obtain

$$\frac{dI_{ion}}{dt} = \frac{-\frac{I_{ion} \times M_o \times 10^6}{2FM_{melt}}}{\frac{2C_rFR_{total}}{RT}K + \frac{M_o \times 10^6}{2\alpha AF\rho_{melt}} + \frac{dC_r}{dI_{ion}}K} \quad [13]$$

where $K = \exp\left(\frac{2FI_{ion}R_{total}}{RT}\right)$

Eq.[13] depicts the variation of the ionic current as a function of time. Thus, if the ionic current can be determined from the measured external short circuit current during

the deoxidation experiments, the entire process can be analyzed/modeled and the validity of the theoretical analysis checked.

CHAPTER 5

RESULTS AND DISCUSSION

From the equivalent circuit shown in Fig 2, the following relationship between the external current and the ionic current can be derived.

$$I_{ex} = I_{ion} \times \frac{R_e}{R_e + R_{ex}} \quad [14]$$

where $R_{ex} = \frac{E_m}{I_{ex}}$

E_m = Open circuit EMF (Volts). Derivation of the formula to calculate R_{ex} is shown in Appendix A.

In our experimental conditions $R_{ex} \approx 3 - 4\Omega$. The low external resistance indicates that the molybdenum-zirconia cermet is a good electrical conductor, and has good adherence to the zirconia tube. K.C.Chou et. al. [20] analyzed nickel-zirconia cermets prepared in a similar manner, and found that the cermet was porous, electrically conducting, and had good adherence to the zirconia tube.

From eqs.[13] and [14] and assuming that R_e and R_{ex} are relatively constant during the experiment, one can also write:

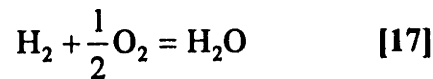
$$\frac{dI_{ex}}{dt} = \frac{\frac{I_{ex} \times M_o \times 10^6}{2FM_{melt}}}{\frac{2C_rFR_{total}}{RT} K_2 + \frac{M_o \times 10^6}{2\alpha AF\rho_{melt}} + \frac{dC_r}{dI_{ex}} \left[\frac{R_e}{R_e + R_{ex}} \right] K_2} \quad [15]$$

where $K_2 = \exp \left[\frac{2FI_{ex}R_{total} \frac{R_e + R_{ex}}{R_e}}{RT} \right]$

In addition, C_r can be calculated utilizing the following formula (derivation of this formula is given in Appendix B)

$$C_r = \frac{K_s \times RT_2}{V \times 1.01 \times 10^5 \times K_P} \times \left[N_{H_2O(i)} + \frac{30I_{ex} \frac{R_c + R_{ex}}{R_c}}{F} \right] \quad [16]$$

where K_s = Sievert's constant, T_2 = room temperature (K), V = flow rate of reducing gas (m^3/min), $N_{H_2O(i)}$ = flow rate of water vapor in the reducing gas (moles/min), and K_P = equilibrium constant for the following equation:



To calculate the equilibrium constant, the thermodynamic data from Kubaschewski et.al. [21] is used.

When the current is small, the current dependent terms in the denominator of eq.[15] become negligible, and it can be rewritten as:

$$\frac{dI_{ex}}{dt} = -\frac{I_{ex} \alpha A \rho_{melt}}{M_{melt}} \quad [18]$$

Integrating eq.[18] gives

$$\ln(I_{ex}) - \ln(I_{ex}^o) = -\frac{\alpha A \rho_{melt}}{M_{melt}} (t - t_o) \quad [19]$$

where I_{ex}^o = short circuit external current (Amperes) at time t_o (min.).

Using experimental values of the external current, eq.[19] can be used to calculate the mass transfer coefficient of oxygen in steel melts.

Plots of $\ln(I_{ex})$ versus time for four deoxidation experiments (A-D) are shown in Fig 6-9. As can be seen from the figures, eq.[19] has a good fit with the experimental values. The regression coefficient obtained for these four experiments is in the range 0.98-0.99. The value for the mass transfer coefficient for the experiments A-D, along with other experimental parameters are given in Table 1. The very minor fluctuations in the mass transfer coefficient for the different experiments is probably due to the fact that the amount of induction stirring in the steel is dependent on its position within the induction coils of the furnace. As can be seen in Table 1, the temperature for experiment A-C is 1873 K. In order to see the effect of temperature on the mass transfer coefficient, experiment D was performed at a temperature of 1893 K. However, the mass transfer coefficient remained in the same range as the other experiments, suggesting that the activation energy is not very large.

Eq. [15] can be used to model the external current versus time curve. The values for α and R_{ex} for the deoxidation experiments are listed in Table 1. The value for R_{ion} ($\sigma_{ion} \approx 2 \times 10^{-3} \Omega^{-1}m^{-1}$) is obtained from the literature [22]. By assuming different values for R_e , and using one experimental value of I_{ex} at any given time, it is possible to solve eq.[15] and model the short circuit current versus time curve. The value of R_e that best fits the short circuit (external) current versus time curve is reported in Table 1. The modeled external current versus time curve is superimposed over the experimental curve in Fig 10a-13a. It can be seen that the actual and the modeled curves agree well with each other. The close match between the actual and the modeled external current curves shows that the assumption made in eq.[15] that R_e does not fluctuate much during the course of the experiment is justified, and a mean value for R_e can be used. Since R_e is known to vary as $(P_{O_2})^{-\frac{1}{4}}$ [23-27], this means that during the course of the experiment $(P_{O_2})^{-\frac{1}{4}}$

across the electrolyte does not vary significantly. Using the mean value of R_e , the ionic transport number can be calculated by the formula

$$t_{ion} = \frac{\sigma_{ion}}{\sigma_e + \sigma_{ion}} = \frac{R_e}{R_e + R_{ion}} \quad [20]$$

where σ_e = electronic conductivity ($\Omega^{-1}m^{-1}$). Using eq.[20], it is calculated that $t_{ion} \approx 0.8$.

By analyzing eq. [15] with respect to Fig. 10a-13a, it is seen that the flat portion of the external current versus time curve (zone 1) is controlled by total resistance of the electrolyte, R_{total} . The region in the external current versus time curve characterized by an exponential decay (zone 2) is controlled by the mass transfer coefficient of oxygen in steel. By using eq. [14] and the modeled external current versus time curve it is also possible to plot the ionic current versus time curve. The ionic current versus time curves for experiment A-D are shown in Fig 10b-13b.

The initial oxygen concentration in the steel melt (C_o), is found from the oxygen analysis of the steel pin sample. Using this value of C_o , Eq.[8] and the ionic current versus time curves shown in Fig 10b-13b, the variation in oxygen concentration in the melt as a function of time is determined for all the experiments (Fig 14-Fig 17). As can be seen from the figures, the modeled curves agree well with the final oxygen analysis of the steel pin samples. The steel pin samples were analyzed by Allegheny Ludlum Corporation (they used the Leco Combustion method for oxygen analysis and their accuracy range was 3-10 ppm of oxygen). The reason for taking only two steel samples per experiment was to minimize the fluctuation in the thermal equilibrium.

TABLE 1. Some Deoxidation Experimental Parameters and Calculated

Mass Transfer Coefficients.

Experiment	Weight of Steel Melt (kg)	Temperature (K)	Electrode/ electrolyte interfacial area (m ²)	N _{H₂O} (i) (moles/min)	R _{ex} (ohms)	R _c (ohms)	Flow rate of reducing gas (ml/min)	Mass Transfer Coefficient α (m/s).
A	0.775	1873	9.25x10 ⁻⁴	5.1x10 ⁻⁶	3.2	0.57	200	1.52x10 ⁻⁵
B	0.699	1873	9.51x10 ⁻⁴	5.1x10 ⁻⁶	2.75	0.56	200	4.83x10 ⁻⁶
C	0.746	1873	11.1x10 ⁻⁴	4.3x10 ⁻⁶	4.2	0.59	300	9.99x10 ⁻⁶
D	0.763	1893	10.8x10 ⁻⁴	5.1x10 ⁻⁶	3.95	0.7	200	4.23x10 ⁻⁶

Constant Experimental Parameters:

Flow rate of inert gas--- 3000 ml/min Ar + 100 ml/min Forming gas

 $\rho_{\text{melt}} = 7100 \text{ kg/m}^3$ [28]

Fig. 6 Calculation of Mass Transfer Coefficient for Experiment A

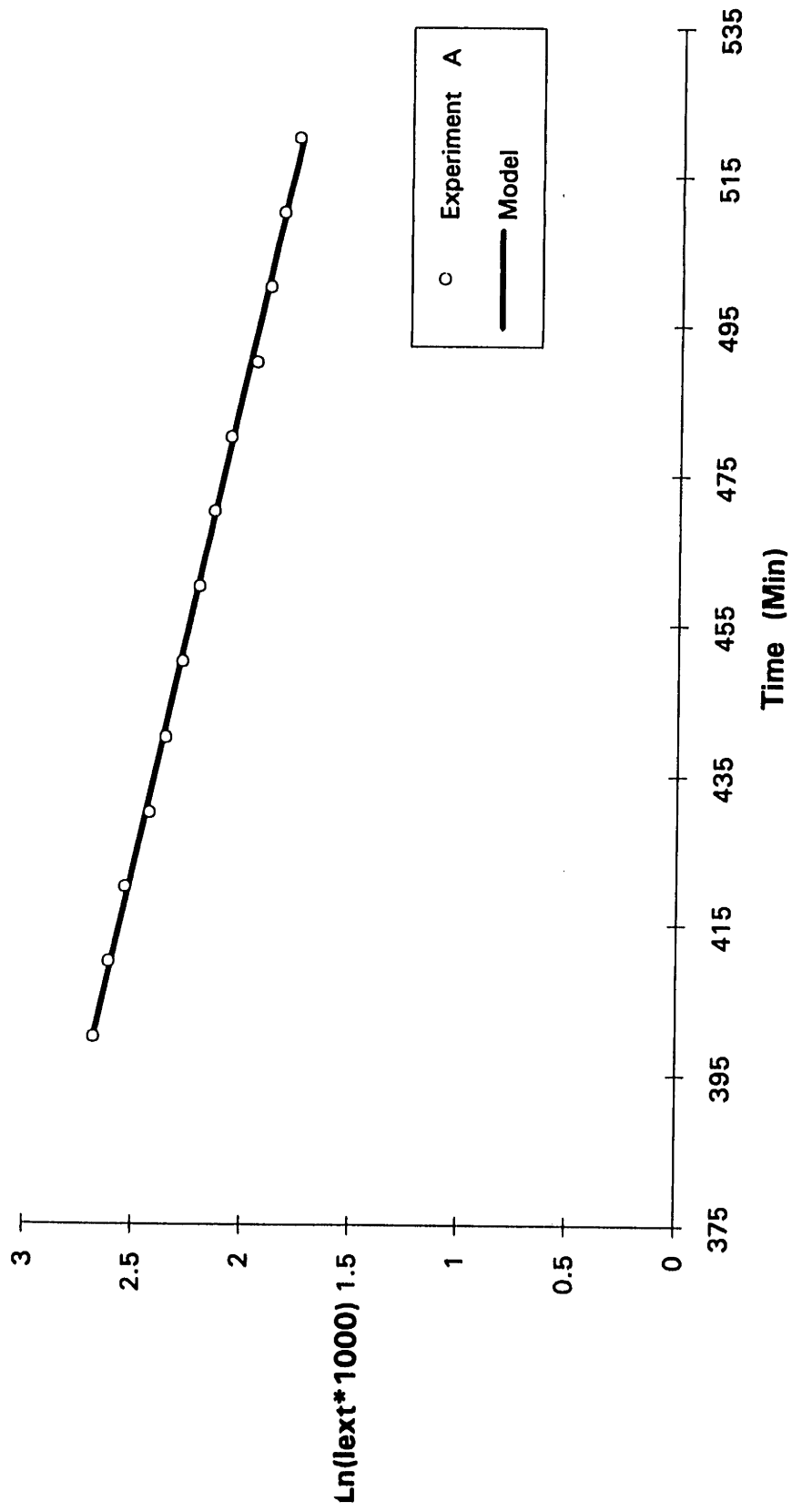


**Fig 7. Calculation of the Mass Transfer Coefficient
for Experiment B**

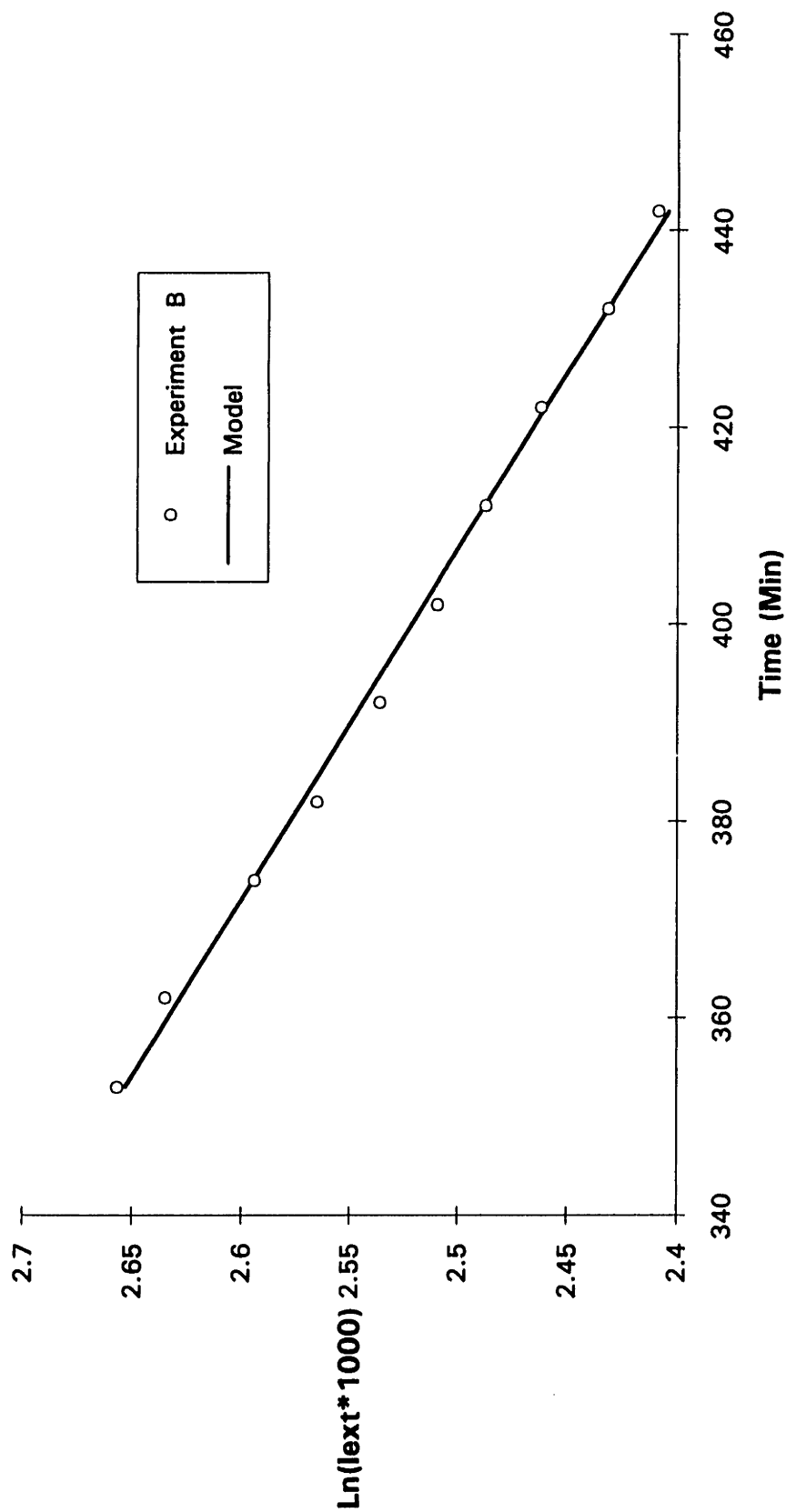


Fig 8. Calculation of Mass Transfer Coefficient for Experiment C

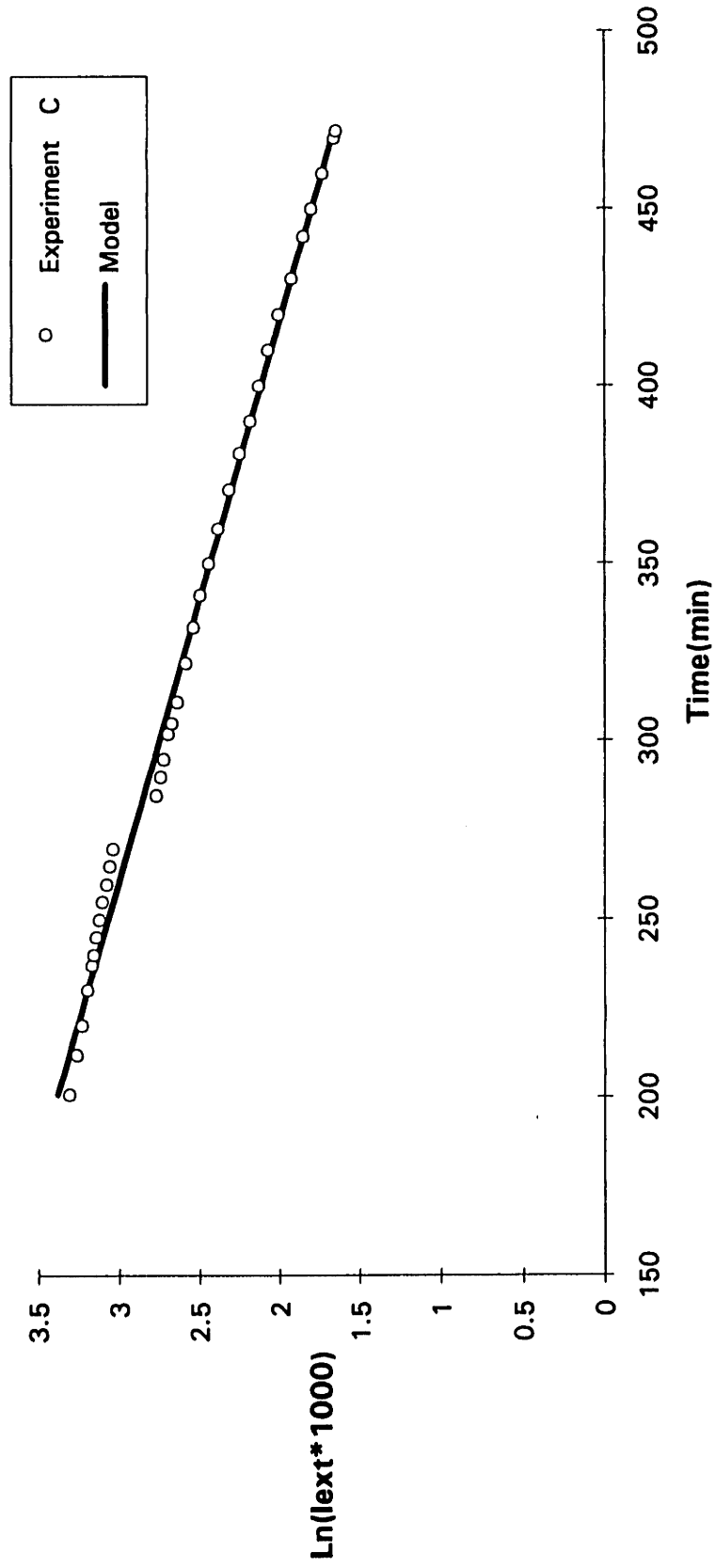
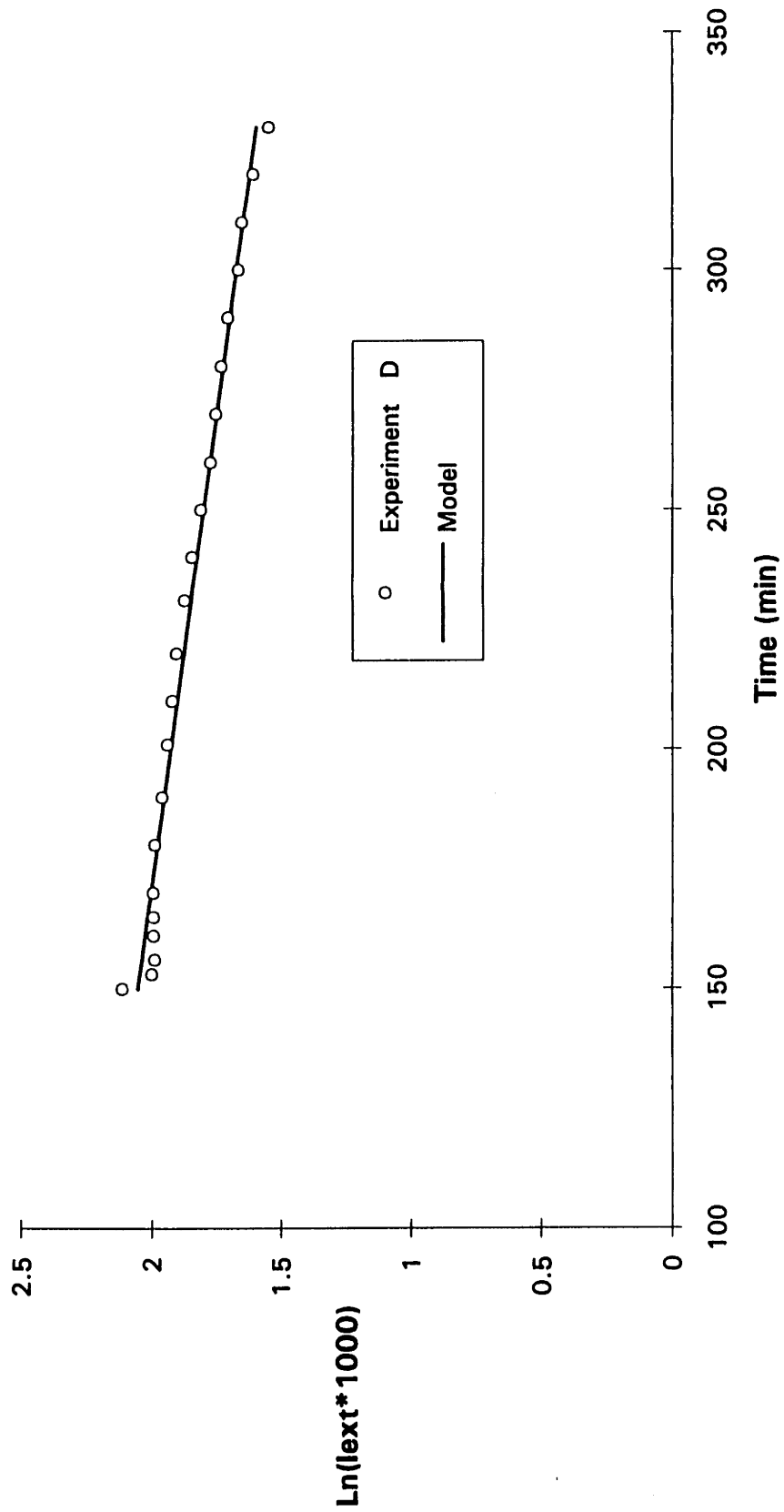


Fig 9. Calculation of Mass Transfer Coefficient for Experiment D



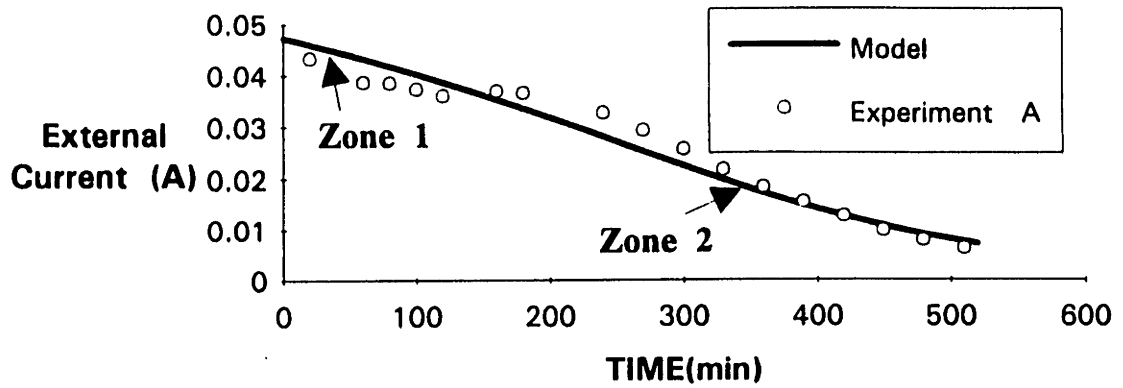


Fig 10a. External Current vs. time curve for Experiment A

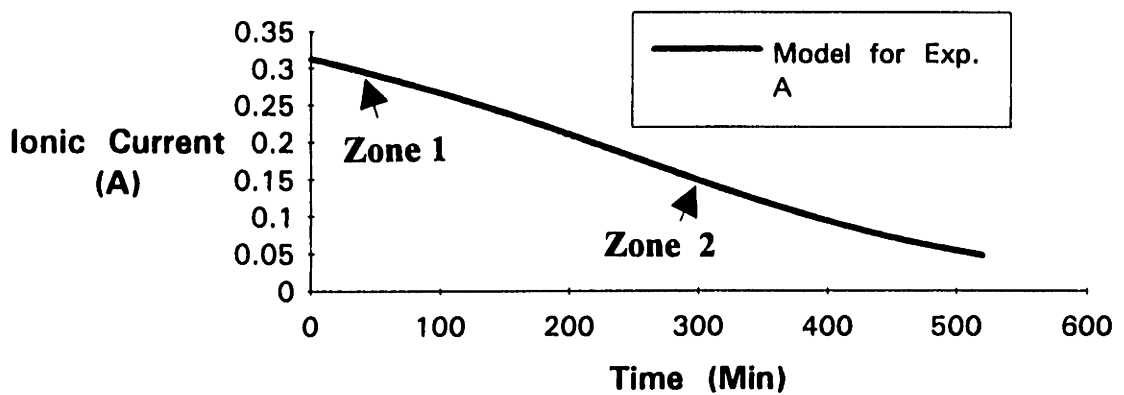


Fig 10b. Ionic Current vs. time curve for Experiment A

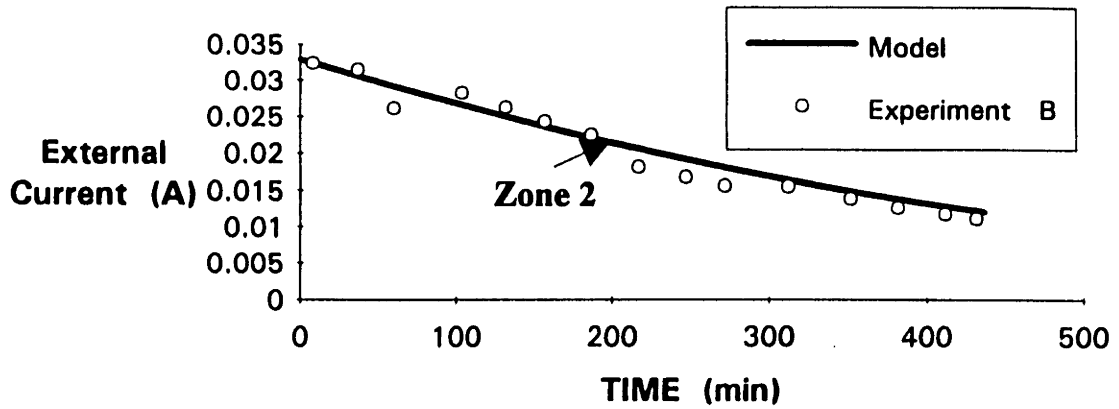


Fig 11a. External Current vs. time curve for Experiment B

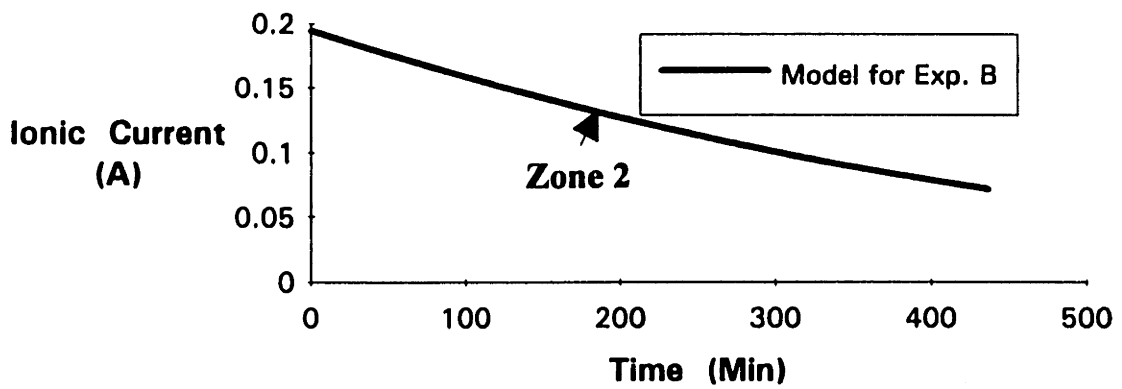


Fig 11b. Ionic Current vs. time curve for Experiment B

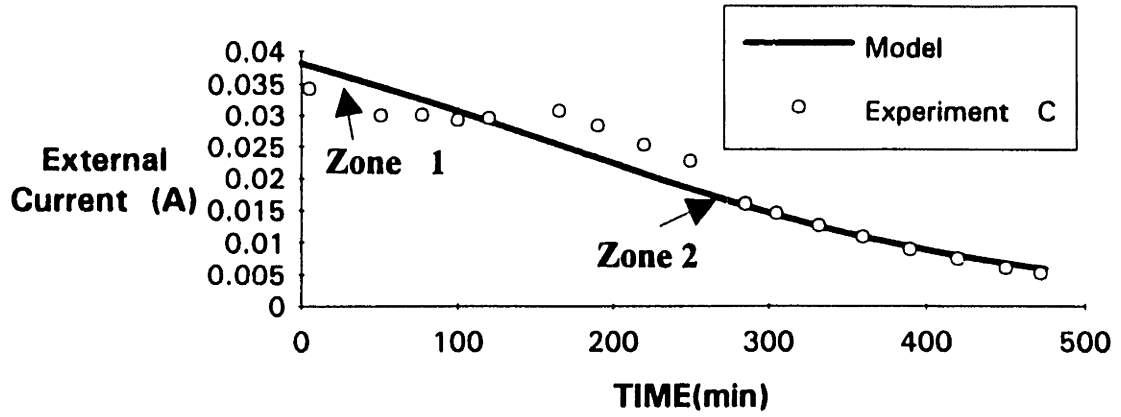


Fig 12a. External Current vs. time curve for Experiment C

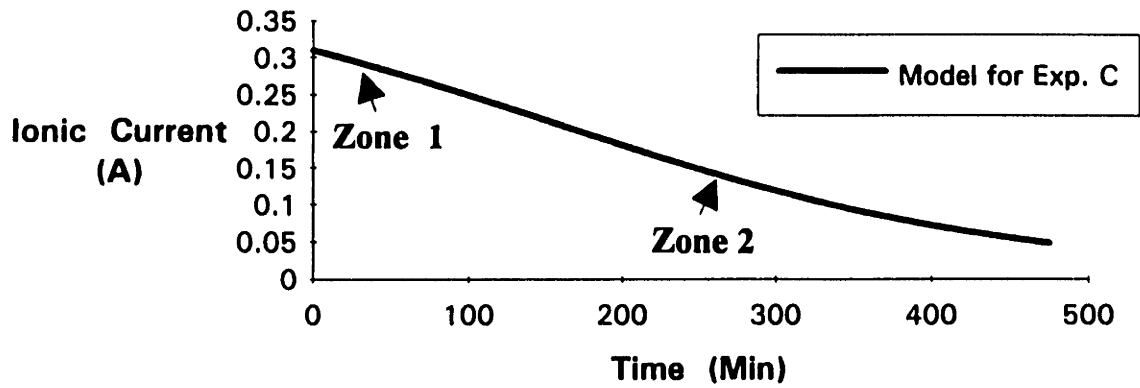


Fig 12b. Ionic Current vs. time curve for Experiment C

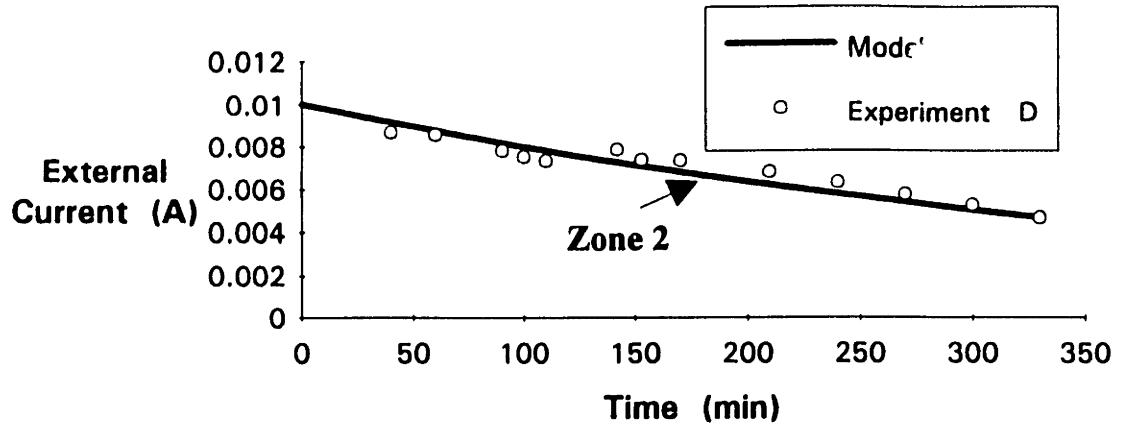


Fig 13a. External Current vs. time curve for Experiment D

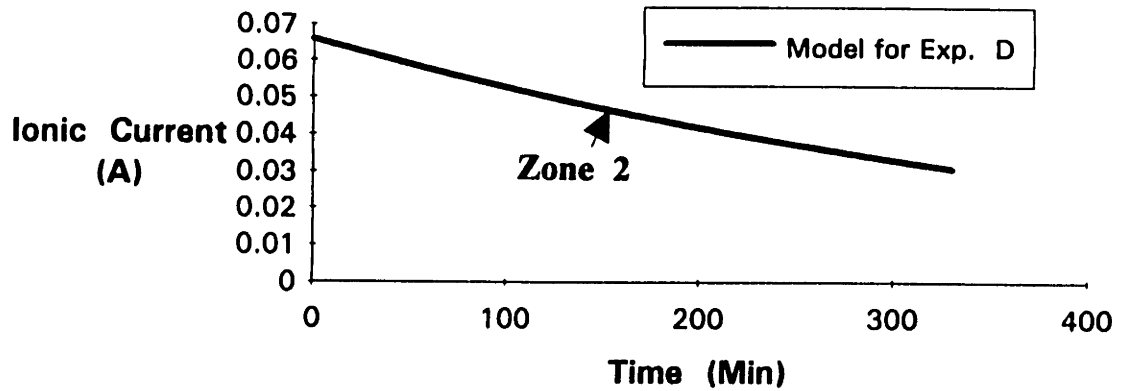


Fig 13b. Ionic Current vs. time curve for Experiment D

Fig 14. Oxygen Removal from Steel Melts (Exp. A)

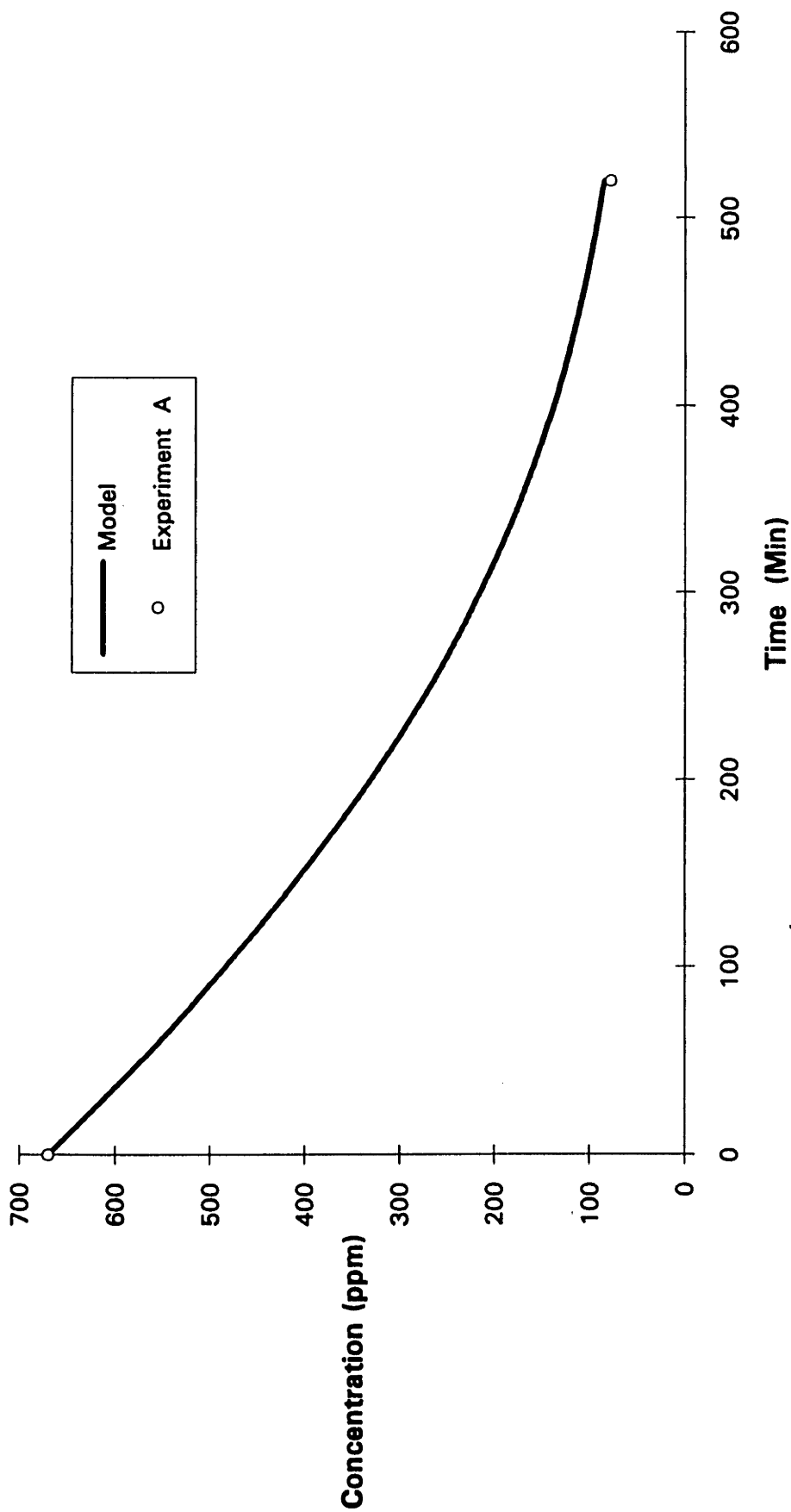


Fig 15. Oxygen Removal from Steel Melts (Exp. B)

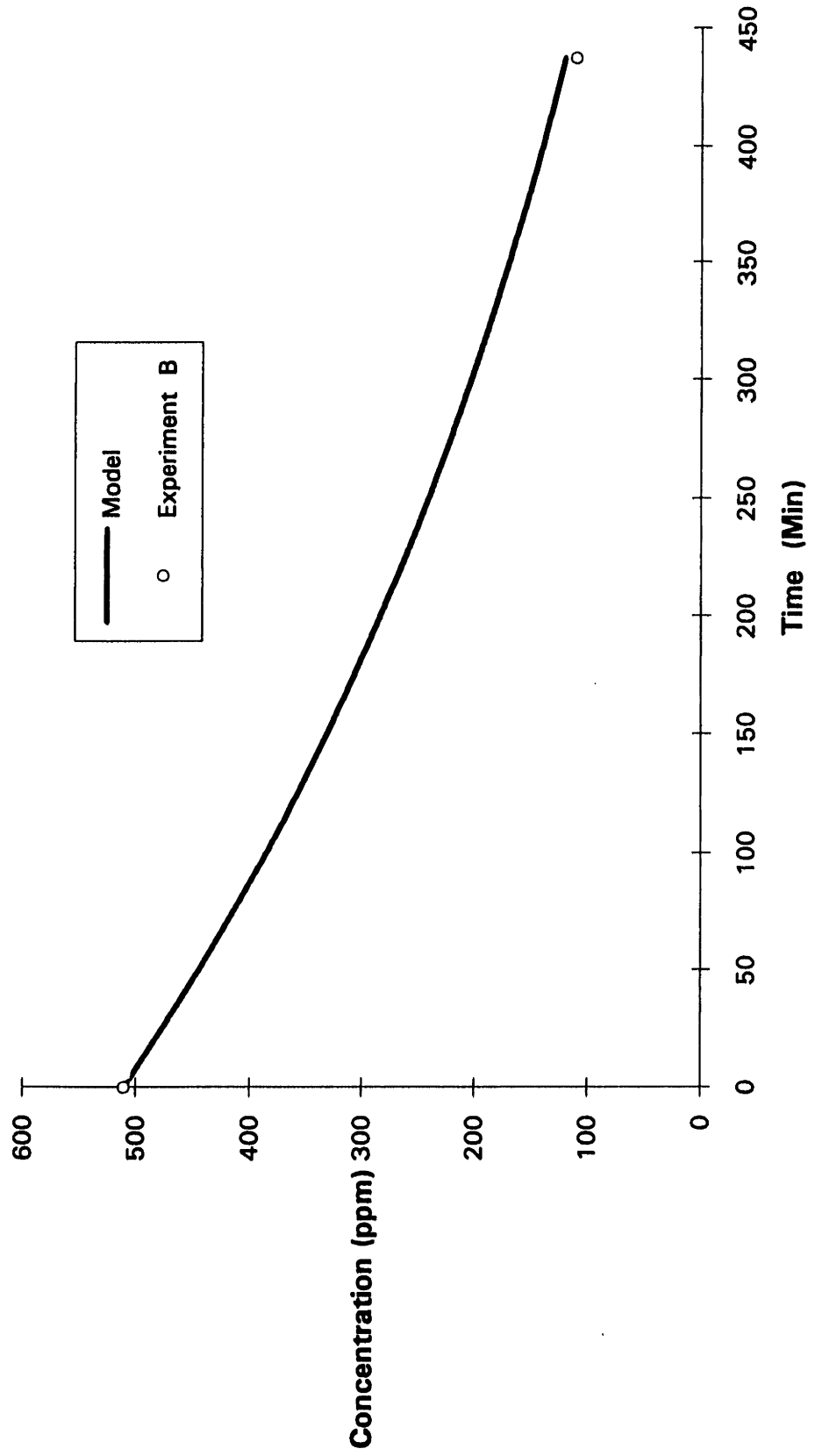


Fig 16. Oxygen Removal from Steel Melts (Exp. C)

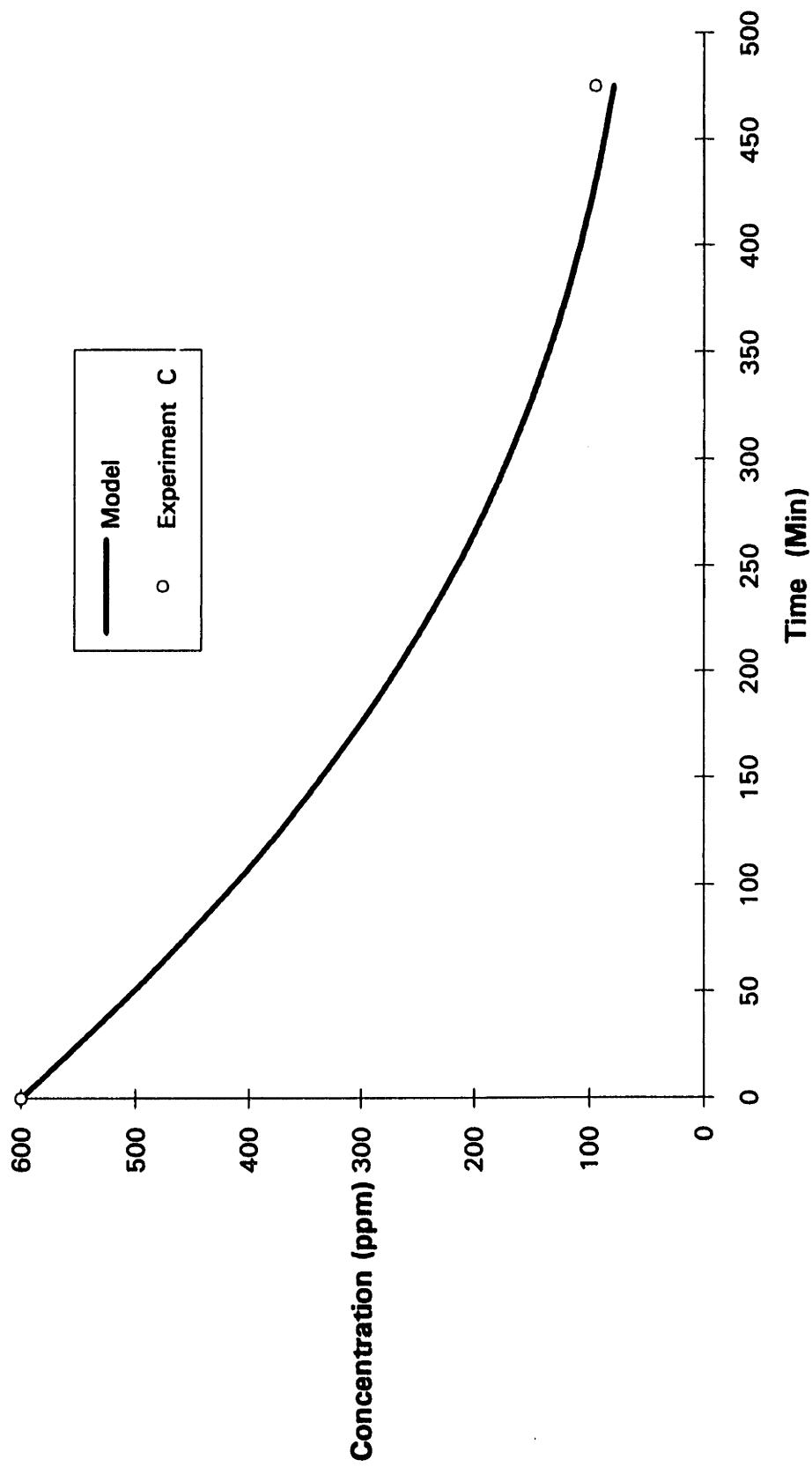
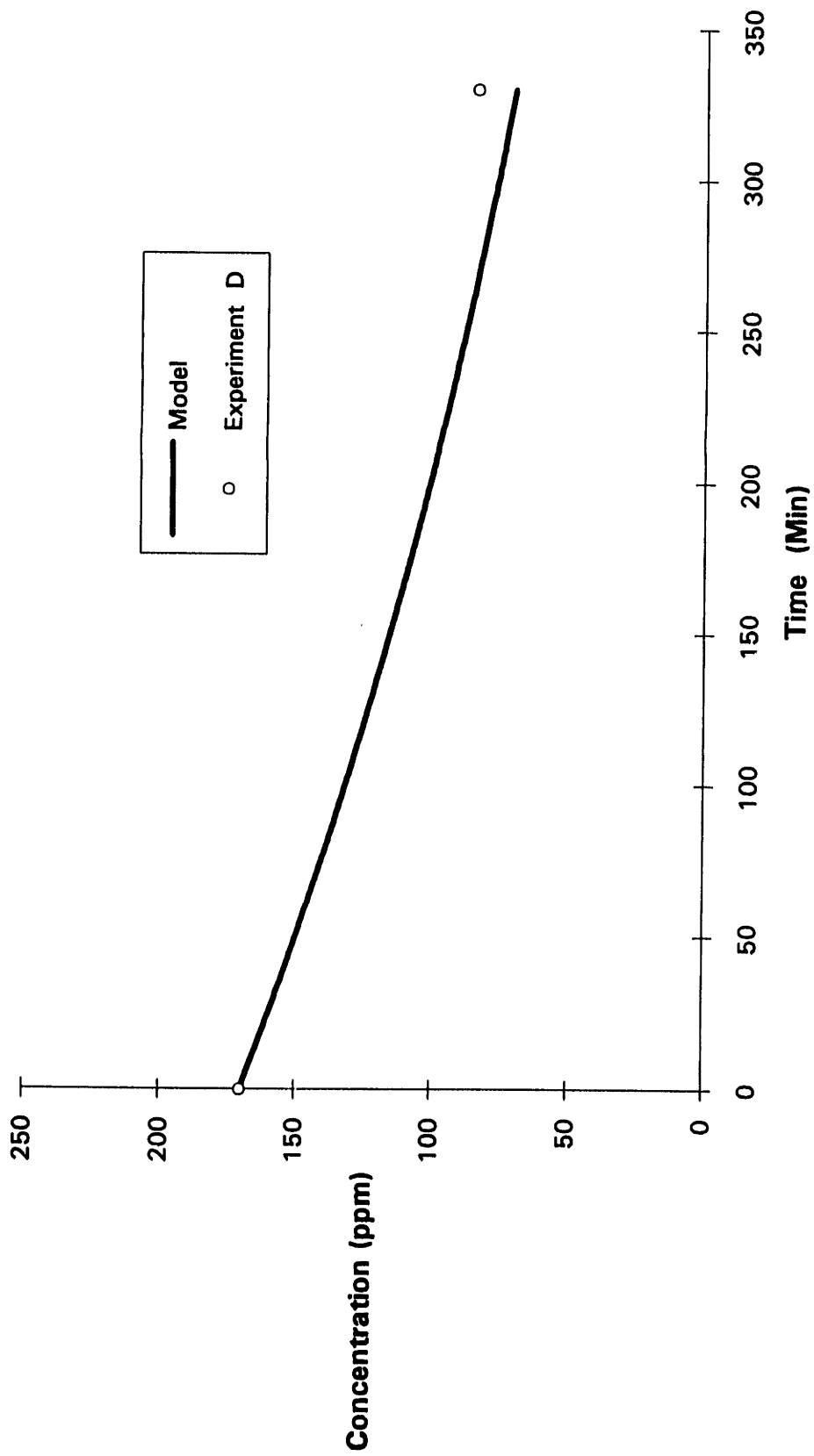


Fig 17. Oxygen Removal from Steel Melts (Exp. D)



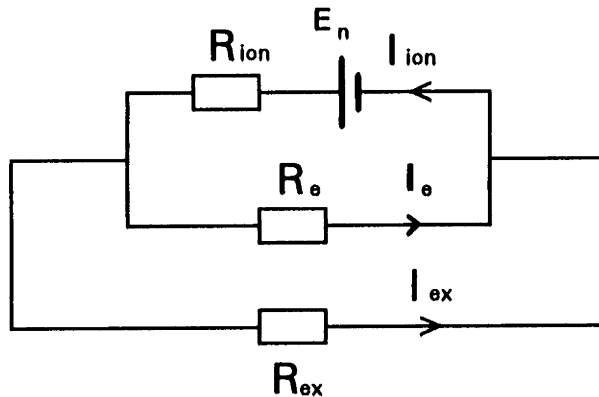
CHAPTER 6

SUMMARY AND CONCLUSION

In this thesis we have demonstrated the feasibility of deoxidizing steel melts by short circuiting a solid electrolyte cell. The solid electrolyte cell consists of a one-end-closed yttria stabilized zirconia tube. This tube is coated with a molybdenum-zirconia cermet, and is inserted into the steel melt. A reducing gas is blown inside the tube, and the molybdenum-zirconia cermet is then short circuited with the steel melt. The deoxidation process is analyzed, and mathematically modeled. It is found that the short circuit external current versus time curve has two distinct zones. In zone 1, the current is leveled and is controlled by the total resistance (R_{total}) of the short circuited cell. In zone 2, the current decreases exponentially, and is controlled by the mass transfer coefficient of oxygen in the melt. The deoxidation kinetics can be enhanced by increasing the mass transfer coefficient of oxygen in the melt (by increasing the stirring intensity in the melt) and by decreasing the total resistance (R_{total}) of the short circuited cell.

APPENDIX A

Considering **SHORT CIRCUIT** conditions



where E_n = Nernst Potential (V)

$$I_{ion} = I_e + I_{ex} \quad [A]$$

$$E_n = I_e R_e + I_{ion} R_{ion} \quad [B]$$

$$E_n = I_{ion} R_{ion} + I_{ex} R_{ex} \quad [C]$$

Subtracting eq.[B] from eq.[C] gives

$$I_{ex} R_{ex} = I_e R_e \quad [D]$$

Multiplying eq.[A] by R_{ion} gives

$$I_{ion} R_{ion} = I_{ex} R_{ion} + I_e R_{ion} \quad [E]$$

Substituting eq.[E] into eq.[B] gives

$$E_n = I_e R_e + I_e R_{ion} + I_{ex} R_{ion} \quad [F]$$

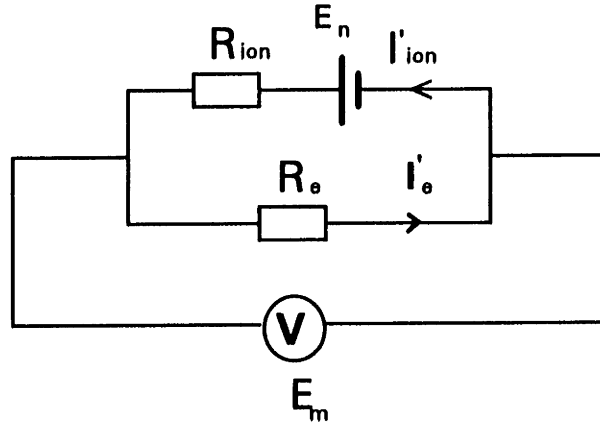
Substituting eq.[D] into eq.[F] gives

$$E_n R_e = I_{ex} [R_e R_{ex} + R_e R_{ion} + R_{ex} R_{ion}] \quad [G]$$

Eq.[G] can be rearranged to the following form

$$I_{ex} = \frac{E_n R_e}{R_e R_{ex} + R_e R_{ion} + R_{ex} R_{ion}}$$

Considering OPEN CIRCUIT conditions



where E_m = Open circuit EMF (V)

$$I'_e R_e = E_m \quad [H]$$

$$I'_e R_e + I'_{ion} R_{ion} = E_n \quad [I]$$

$$I'_e = I'_{ion} \quad [J]$$

$$E_m = E_n - I'_{ion} R_{ion} \quad [K]$$

Using eq.[I] and eq.[J],

$$E_n = I'_{ion} (R_{ion} + R_e) \quad [L]$$

Using eq.[K] and eq. [L],

$$E_n = E_m \left(\frac{R_{ion} + R_e}{R_e} \right) \quad [M]$$

Combining Short Circuit and Open Circuit equations

Using eq.[G] and eq.[M]

$$I_{ex} = \frac{E_m}{R_{ex} + \left(\frac{R_e R_{ion}}{R_e + R_{ion}} \right)} \quad [N]$$

Since the external resistance (R_{ex}), is much larger than the ionic resistance of the electrolyte cell (R_{ion}),

$$\frac{1}{R_{ion}} \gg \frac{1}{R_{ex}}$$

$$\frac{1}{R_e} + \frac{1}{R_{ion}} \gg \frac{1}{R_{ex}}$$

$$R_{ex} \gg \frac{1}{\frac{1}{R_e} + \frac{1}{R_{ion}}}$$

$$\text{Therefore, } R_{ex} \gg \frac{R_e R_{ion}}{R_e + R_{ion}}$$

Using this relationship, eq.[N] can be approximated to the following form

$$R_{ex} = \frac{E_m}{I_{ex}}$$

APPENDIX B

Derivation of formula for C_r under short circuit conditions

	H₂	+	1/2 O₂	=	H₂O
Initial no. of moles/min	N _{H2(i)}		N _{O2(i)}		N _{H2O(i)}
Immediately after short circuit	N _{H2(i)}		N _{O2(i)} +N _{O2(s.c.)}		N _{H2O(i)}
Equilibrium after short circuit	N _{H2(i)} -2X		N _{O2(i)} +N _{O2(s.c.)} -X		N _{H2O(i)} +2X
Total number of moles = N _T = N _{H2(i)} +N _{H2O(i)} +N _{O2(i)} +N _{O2(s.c.)} -X					

$$K_P = \frac{P_{H_2O}}{P_{H_2} \times (P_{O_2})^{\frac{1}{2}}} = \frac{(N_{H_2O(i)} + 2X)(N_T)^{\frac{1}{2}}}{(N_{H_2(i)} - 2X)[N_{O_2(i)} + N_{O_2(s.c.)} - X]^{\frac{1}{2}}}$$

where K_P = equilibrium constant.

As K_P is large (at 1600°C), and the hydrogen gas relatively pure, therefore

$$N_{O_2(s.c.)} \gg N_{O_2(i)}, \quad X \approx N_{O_2(s.c.)}$$

In addition, as $N_{H_2(i)} \gg 2X$, the equilibrium constant can be modified to the following form:

$$K_P = \frac{[N_{H_2O(i)} + 2N_{O_2(s.c.)}]}{(N_{H_2(i)})(P_{O_2}^f)^{\frac{1}{2}}}$$

where $P_{O_2}^f$ = oxygen partial pressure in the reducing gas.

In addition, $N_{O_2(s.c.)} = \frac{60I_{ion}}{4F}$, and $N_{H_2(i)} = \frac{RT_2}{V \times 1.01 \times 10^5}$ where V is the volume in m^3/min and T_2 is the room temperature (K)

Therefore,

$$(P_{O_2}^f)^{\frac{1}{2}} = \frac{RT_2}{V \times 1.01 \times 10^5 \times K_P} \times [N_{H_2O(i)} + \frac{30I_{ion}}{F}], \text{ and}$$

$$C_r = \frac{K_s \times RT_2}{V \times 1.01 \times 10^5 \times K_p} \times \left[N_{H_2O(i)} + \frac{30I_{ion}}{F} \right]$$

where C_r = oxygen concentration in the reducing gas, and K_s = Sievert's constant.

From equivalent circuit diagram (Fig 2),

$$I_{ion} = I_{ex} \left[\frac{R_e + R_{ex}}{R_e} \right]$$

Therefore,

$$C_r = \frac{K_s \times RT_2}{V \times 1.01 \times 10^5 \times K_p} \left[N_{H_2O(i)} + \frac{30I_{ex} \left(\frac{R_e + R_{ex}}{R_e} \right)}{F} \right]$$

BIBLIOGRAPHY

1. W. Nernst, Z. Elektrochem., **6**, 1900, p41
2. C. Wagner, Naturwissenschaften, **31**, 1943, p265
3. F. Hund, Z. Physik. Chem., **199**, [1-3], 1952, p142
4. K. Kiukkola and C. Wagner, J. Electrochem. Soc., **104**, [6], 1957, p379
5. W.D. Kingery, J. Pappis, M.E.Doty and D.C. Hill, J. Am. Ceram. Soc., **42**, [8], 1959, p393
6. J. Weissbart and R.Ruka, J. Electrochem. Soc., **109**, [8], 1962, p723
7. P. H. Scaife, D.A. Swinkels, and S.R. Richards, High Temperature Science, **8**, 1976, p31
8. M. Kleitz, E. Fernandez, J. Fouletier, and P. Fabry, in " Advances in Ceramics-Science and Technology of Zirconia, 3", ed. A.H. Heuer and L.W.Hobbs, The American Ceramic Society, Inc., 1981, p349
9. M. Iwase, E. Ichise, M. Takeuchi, and T. Yamasaki, Transaction of the Japan Institute of Metals, **25**, 1984, p43
10. M.J.U.T. Van Wijngaarden, J.M.A.Geldenhuis, and R.J.Dippenaar, J. S. Afr. Inst. Min. Metall., **88**, 1988, p265
11. B.Korousic and B.Marincek, Helv.Chim.Acta, **51**, 1968, p907
12. W.A.Fischer and D.Janke, Scripta Metallurgica, **6**, 1972, p923
13. Karl E. Oberg, Lawrence M. Friedman, William M. Boorstein , and Robert A. Rapp, Metallurgical Transactions, **4**, 1973, p75
14. T. H. Etsell, unpublished research, University of Toronto
15. M. Iwase, unpublished research, University of Toronto
16. M. Iwase, M.Tanida, A. Mclean, and T.Mori, Metallurgical Transaction, **12B**, 1981, p517
17. J. C. Chan, C.B. Alcock, and K.T. Jacob, Canadian Metall. Quart., **12**, 1973, p439
18. N.J.Maskalick, Proceedings of the First International Symposium on Solid Oxide Fuel Cells, e.d. S.C.Singhal, , the Electrochemical Society, Inc., 1993, p279
19. J.F.Elliott, Molly Gleiser, and V. Ramakrishna, Thermochemistry for Steel Making, **2**, , 1963, p618
20. K.C.Chou, S.Yuan, and U.B.Pal, Proceedings of the Third International Symposium on Solid Oxide Fuel Cells, ed. S.C.Singhal, H.Iwahara, , The Electrochemical Society, Inc., (1993), p431
21. O. Kubaschewski, E.LL. Evans, and C.B.Alcock, Metallurgical Thermochemistry, Fourth Edition, 1965, p424
22. Sotomitsu Ikeda, Osamu Sakurai, Keizo Uematsu, Nobuyasu Mizutani and Masanori Kato, Journal of Material Science, **20**, 1985, p4593
23. A.W.Smith, F.W.Mezzaros, and C.D.Amata, J.Am.Ceram.Soc., **49**, 1966, p240
24. J.W.Patterson, E.C.Bogren, and R.A.Rapp, J.Electrochem.Soc., **114**, 1967, p752
25. W.A.Fischer, Fast Ion Transport in Solids, edited by W.Van Gool., 1973, p503
26. S.F.Pal'guev, V.K.Gil'derman, and A.D.Neuimin, J. Electrochem. Soc., **122**,

1975, p745

27. M.Iwase and T.Mori, *Met. Trans.*, **9B**, 1978, p365

28. C.Benedicks, N.Ericsson, and G.Ericson, *Arch. Eisenhüttenw.*, **3**, 1929-1930, p473

BIOGRAPHICAL NOTE

The author was born in Karachi, Pakistan. He did his O' Level (Cambridge University Examination) and A' Level (Cambridge University Examination) from Karachi Grammer School. He joined University of Pennsylvania in September 1988, and graduated from there in May 1992, with a B.S.E. in Material Science and Engineering, and a B.S.Econ. in Entrepreneurial Management. He joined the Master's program in Material Science and Engineering at Massachusetts Institute of Technology in September 1992.